PRAMANA — journal of physics
© Indian Academy of Sciences
Vol. 85, No. 1
July 2015
pp. 125–148

Simultaneous effects of Hall and convective conditions on peristaltic flow of couple-stress fluid in an inclined asymmetric channel

T HAYAT[1,2], MARYAM IQBAL[1], HUMAIRA YASMIN[1,*], FUAD E ALSAADI[2] and HUIJUN GAO[3]

[1]Department of Mathematics, Quaid-I-Azam University 45320, Islamabad 44000, Pakistan
[2]Department of Electrical and Computer Engineering, Faculty of Engineering, King Abdulaziz University, Jeddah 21589, Saudi Arabia
[3]Research Institute of Intelligent Control and Systems, Harbin Institute of Technology, Harbin, 150080, People's Republic of China
*Corresponding author. E-mail: qau2011@gmail.com

MS received 6 September 2013; revised 24 February 2014; accepted 16 June 2014
DOI: 10.1007/s12043-014-0888-1; ***e*Publication:** 25 January 2015

Abstract. A mathematical model is developed to analyse the peristaltic flow of couple-stress fluid in an inclined asymmetric channel with convective conditions. Soret and Dufour and Hall effects are taken into account. Analysis has been carried out in a wave frame of reference. Expressions for velocity, pressure gradient, temperature and concentration are constructed. Pumping and trapping phenomena are examined. Impact of sundry parameters on the velocity, temperature and concentration is discussed.

Keywords. Couple stress fluid; convective conditions; Hall effect; inclined channel.

PACS No. 47.50.−d

1. Introduction

The study of peristaltic pumping of fluids generated by a progressive wave of area concentration or expansion along the length of distensible tube is significant in physiological and industrial processes. Many physiological fluids like urine from kidney to bladder through ureters, food material through the digestive tract, semen in vas deferens, spermatozoa in ductus efferentes, blood circulation in small blood vessels, cilia movement, bile flow, etc. obey the principle of peristalsis. The process of peristaltic mechanism is also useful in heart lung machine, dialysis machine, roller and finger pumps and noxious fluid transport in nuclear industry. Ample investigations for peristalsis have been made in view of aforementioned applications. Such analyses have been carried out under one or more simplified assumptions of large wavelength, small amplitude ratio, small Reynolds

number and small wave number (see recent attempts [1–11] and several related studies therein). The interaction of peristalsis with heat transfer is quite obvious in the oxygenation and hemodialysis processes. Simultaneous effects of heat and mass transfer cannot be ignored in heat convection due to blood flow through the pores of tissues and metabolic heat generation and external interactions such as electromagnetic radiation from cell phones. Magnetohydrodynamic (MHD) character of fluid is important in MHD power generators, metallurgical process, magnetic resonance imaging (MRI), magnetic devices, magnetic particles as the drug carriers, in cancer tumour treatment and also to reduce bleeding during surgeries. Hence, several researchers discussed the peristaltic transport of fluid through MHD/heat and mass transfer aspects. A few representative contributions in this direction can be seen in [12–20].

When heat and mass transfer occur simultaneously in a moving fluid, the relations between the fluxes and the driving potentials are of more intricate nature. It has been observed that an energy flux can be generated not only by the temperature gradient but also by the concentration gradient. The energy flux caused by a concentration gradient is termed as the diffusion-thermo (Dufour) effect. On the other hand, mass fluxes can also be created by temperature gradients and this embodies the thermo diffusion (Soret) effect. In most of the studies related to heat and mass transfer process, Soret and Dufour effects are neglected their magnitude is smaller than the effects described by the Fourier's (defines the thermal conductivity of a material) and Fick's (define the diffusion coefficient for species in the mixture) laws. Note that the effects of Soret and Dufour are significant when density differences are present in the flow regime. Another important aspect is related to Hall effect. Such effect cannot be ignored when flow subjected to high magnetic field is considered. It has been noticed that peristalsis in the presence of Hall/Soret and Dufour effects is given very less attention. To our knowledge, only few studies [21–26] are available in this direction. On the other hand, in the past, the peristalsis mostly dealt with the heat transfer effect through either prescribed surface temperature or prescribed heat flux. Only limited information is available about the peristalsis with convective boundary conditions [27,28].

The purpose of the present investigation is three-fold: Firstly, to analyse the effect of inclined magnetic field on peristaltic flow of couple-stress fluid in an inclined channel, secondly to discuss the influence of Hall current and thirdly to examine the flow in an asymmetric channel with convective effects. It is important to consider asymmetric channel because uterine peristalsis resulting from myometrial concentrations can take place in both symmetric and asymmetric directions. Mathematical analysis is presented for large wavelength and low Reynolds number. Flow quantities of interest are analysed in detail for various pertinent parameters.

2. Mathematical modelling and solution

We investigate the peristaltic flow of an incompressible couple-stress fluid in an inclined asymmetric channel. The fluid is electrically conducting in the presence of an inclined magnetic field. The induced magnetic field is neglected for small magnetic Reynolds number. Hence

$$\mathbf{B} = (B_0 \sin\theta,\, B_0 \cos\theta,\, 0). \tag{1}$$

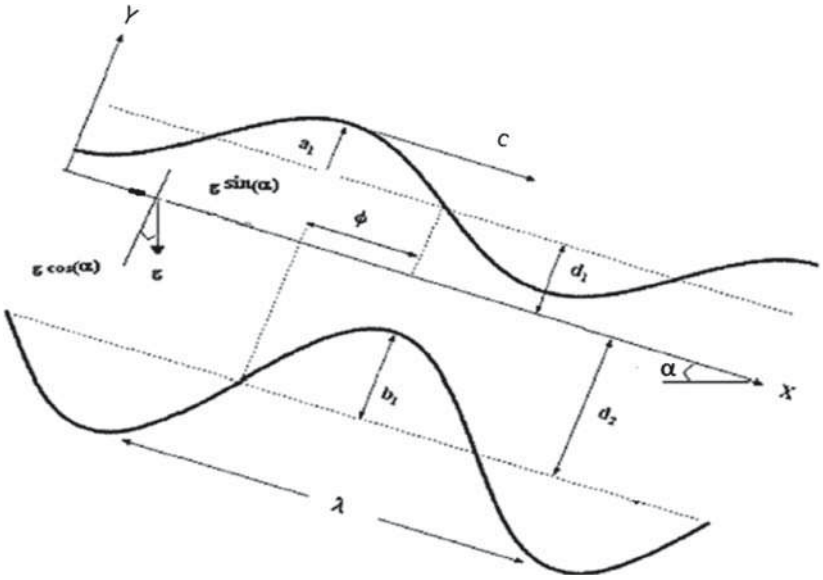

Figure 1. Schematic diagram of the problem.

We consider the Cartesian coordinate system in the laboratory frame $(\bar{X}, \bar{Y}, \bar{t})$. We have the also considered the heat and mass transfer processes in the presence of Soret and Dufour effects. The channel walls satisfy convective boundary conditions. Moreover, the effect of Hall current is taken into account.

Thus, the generalized Ohm's law can be expressed as

$$\mathbf{J} = \sigma^* \left[(\mathbf{V} \times \mathbf{B}) - \frac{1}{en} (\mathbf{J} \times \mathbf{B}) \right], \tag{2}$$

where effect of electrical field is not considered and geometry of the problem is shown in figure 1. From the above equation

$$\mathbf{J} \times \mathbf{B} = \sigma^* (\mathbf{V} \times \mathbf{B}) \times \mathbf{B} - \frac{\sigma^*}{en} [(\mathbf{J} \times \mathbf{B}) \times \mathbf{B}]. \tag{3}$$

Using velocity $\mathbf{V} = (\bar{U}, \bar{V}, 0)$ and eqs (1) and (3), we obtain

$$\mathbf{J} \times \mathbf{B} = \left[\frac{-\sigma^* B_0^2}{1+m^2} \cos\theta (\bar{U} \cos\theta - \bar{V} \sin\theta), \frac{\sigma^* B_0^2}{1+m^2} \sin\theta (\bar{U} \cos\theta - \bar{V} \sin\theta), \right.$$
$$\left. \frac{\sigma^* B_0^2 m}{1+m^2} (\bar{U} \cos\theta - \bar{V} \sin\theta) \right], \tag{4}$$

in which $\mathbf{J}$ is the current density, B_0 is the applied magnetic field, σ^* is the electrical conductivity, $\bar{U}$, $\bar{V}$ are the velocity components in fixed frame, m $(=\sigma^* B_0/en)$ is the Hall parameter, n is the number density of electrons, e is the electric charge and θ is the inclination of the magnetic field.

Under the assumptions of long wavelength and low Reynolds number (Re $\to$ 0) [29,30] mathematical model of the given problem is

$$-\frac{\mathrm{d}p}{\mathrm{d}x}+\frac{\partial^2 u}{\partial y^2}-\eta\frac{\partial^4 u}{\partial y^4}-\frac{M^2}{1+m^2}\cos\theta(u\cos\theta+\cos\theta)+\frac{\mathrm{Re}}{\mathrm{Fr}}\sin\alpha=0, \quad (5)$$

$$-\frac{\partial p}{\partial y}=0, \quad (6)$$

$$\frac{\partial^2\gamma}{\partial y^2}+\mathrm{Br}\left(\frac{\partial u}{\partial y}\right)^2+\eta\mathrm{Br}\left(\frac{\partial^2 u}{\partial y^2}\right)^2+\mathrm{Pr}\,\mathrm{Du}\frac{\partial^2\varphi}{\partial y^2}=0, \quad (7)$$

$$\frac{\partial^2\varphi}{\partial y^2}+\mathrm{Sc}\,\mathrm{Sr}\frac{\partial^2\gamma}{\partial y^2}=0. \quad (8)$$

Clearly eq. (6) implies that $p \neq p(y)$.

The corresponding boundary conditions and wall geometries $h_1(x)$ and $h_2(x)$ in the dimensionless form are given by

$$u=-1,\quad \frac{\partial^2 u}{\partial y^2}=0,\quad \frac{\partial\gamma}{\partial y}+\mathrm{Bi}_1\gamma=0,\quad \varphi=0,$$
$$\text{at}\quad y=h_1(x)=1+a\sin(2\pi x), \quad (9)$$

$$u=-1,\quad \frac{\partial^2 u}{\partial y^2}=0,\quad \frac{\partial\gamma}{\partial y}-\mathrm{Bi}_2\gamma=0,\quad \varphi=1,$$
$$\text{at}\quad y=h_2(x)=-d-b\sin(2\pi x+\phi), \quad (10)$$

where Bi_1 and Bi_2 are the Biot numbers at the upper and lower walls of the channel, $a=a_1/d_1$, $b=a_2/d_1$ and $d=d_2/d_1$ satisfy the condition

$$a^2+b^2+2ab\cos\phi\le(1+d)^2. \quad (11)$$

Detailed simplification of the mathematical model and its corresponding boundary conditions are given in Appendix A. The dimensionless average flux F in the wave frame is defined as

$$F=\int_{h_2}^{h_1}u\,\mathrm{d}y. \quad (12)$$

Dimensionless average flux in the laboratory (σ) and wave (F) frames are related by the following expression:

$$\sigma=F+1+d. \quad (13)$$

The non-dimensional expression for the rise in pressure per wavelength Δp_λ is given by

$$\Delta p_\lambda=\int_0^1\left(\frac{\mathrm{d}p}{\mathrm{d}x}\right)\mathrm{d}x. \quad (14)$$

The closed form solution of eq. (5) is

$$u(y)=C_1\mathrm{e}^{(y/\sqrt{2})M_1}+C_2\mathrm{e}^{-(y/\sqrt{2})M_1}+C_3\mathrm{e}^{(y/\sqrt{2})M_2}+C_4\mathrm{e}^{-(y/\sqrt{2})M_2}-\frac{H\sec^2\theta}{z}, \quad (15)$$

Using eqs (12) and (15) we obtain $\mathrm{d}p/\mathrm{d}x$ in the form

$$\begin{aligned}
\frac{\mathrm{d}p}{\mathrm{d}x} &= \Bigg(-f - h_1 + h_2 + \frac{h_1(1+m^2)R\sec\theta\tan\theta}{\mathrm{Fr}M^2} \\
&- \frac{h_2(1+m^2)R\sec\theta\tan\theta}{\mathrm{Fr}M^2} \\
&- \left(\sqrt{2}A_4\left(\mathrm{e}^{\frac{h_1\sqrt{\frac{-A_3}{\eta}}}{\sqrt{2}}} - \mathrm{e}^{\frac{h_2\sqrt{\frac{-A_3}{\eta}}}{\sqrt{2}}}\right)\left(1+m^2\right)R\sec\theta\tan\theta\right)/ \\
&\left(\left(\mathrm{e}^{\frac{h_1\sqrt{\frac{-A_3}{\eta}}}{\sqrt{2}}} + \mathrm{e}^{\frac{h_2\sqrt{\frac{-A_3}{\eta}}}{\sqrt{2}}}\right)\mathrm{Fr}M^2\sqrt{\frac{-A_3}{\eta}}A_5\right) \\
&- \frac{A_3\left(\mathrm{e}^{A_1} - \mathrm{e}^{A_2}\right)\left(1+m^2\right)R\sec\theta\tan\theta}{\sqrt{2}\left(\mathrm{e}^{A_1} + \mathrm{e}^{A_2}\right)\mathrm{Fr}M^2\sqrt{(A_4/\eta)}A_5} \\
&+ \left(\left(\mathrm{e}^{A_1} - \mathrm{e}^{A_2}\right)\left(1+m^2\right)R\left(A_3 + 2M^2\eta\cos 2\theta + m^2A_3\right)\sec\theta\tan\theta\right)/ \\
&\left(\sqrt{2}\left(\mathrm{e}^{A_1} + \mathrm{e}^{A_2}\right)\mathrm{Fr}M^2\sqrt{\frac{A_4}{\eta}}A_6\right)/\left(\frac{h_1\left(1+m^2\right)\sec^2\theta}{M^2}\right. \\
&- \frac{h_2\left(1+m^2\right)\sec^2\theta}{M^2} - \sqrt{2}A_4\left(\mathrm{e}^{\frac{h_1\sqrt{\frac{-A_3}{\eta}}}{\sqrt{2}}} - \mathrm{e}^{\frac{h_2\sqrt{\frac{-A_3}{\eta}}}{\sqrt{2}}}\right)\left(1+m^2\right)\sec^2\theta/ \\
&\left(\mathrm{e}^{\frac{h_1\sqrt{\frac{-A_3}{\eta}}}{\sqrt{2}}} + \mathrm{e}^{\frac{h_2\sqrt{\frac{-A_3}{\eta}}}{\sqrt{2}}}\right)M^2\sqrt{\frac{-A_3}{\eta}}A_5 - \frac{A_3\left(\mathrm{e}^{A_1} - \mathrm{e}^{A_2}\right)\left(1+m^2\right)\sec^2\theta}{\sqrt{2}\left(\mathrm{e}^{A_1} + \mathrm{e}^{A_2}\right)\mathrm{Fr}M^2\sqrt{(A_4/\eta)}A_5} \\
&+ \left(\left(\mathrm{e}^{A_1} - \mathrm{e}^{A_2}\right)\left(1+m^2\right)\left(A_3 + 2M^2\eta\cos 2\theta + m^2A_3\right)\sec^2\theta\right)/ \\
&\left.\left(\sqrt{2}\left(\mathrm{e}^{A_1} + \mathrm{e}^{A_2}\right)M^2\sqrt{\frac{A_4}{\eta}}A_6\right). \right. \qquad (16)
\end{aligned}$$

Substituting eqs (5) and (15) into eq. (7), the closed form solution of $\gamma(y)$ is given by

$$\begin{aligned}
\gamma(y) &= C_5 + yC_6 + \frac{1}{8(-1+\mathrm{Pr\ Sc\ Sr\ Du})}\mathrm{Bre}^{-\sqrt{2}(M_1+M_2)y} \\
&\times\left(-\mathrm{e}^{\sqrt{2}M_2y}(-3+M_3)C_2^2 + \mathrm{e}^{\sqrt{2}M_1y}(3+M_3)C_4^2\right) \\
&- \frac{1}{(-1+\mathrm{Pr\ Sc\ Sr\ Du})}\mathrm{Br}\ y^2z(C_1C_2 + C_3C_4)\cos^2\theta \\
&- \frac{2}{(M_1-M_2)^2(-1+\mathrm{Pr\,Sc\ Sr\ Du})} \\
&\times \mathrm{Br}\,\mathrm{e}^{(y/\sqrt{2})(-M_1+M_2)}C_2C_3(M_1M_2 - 2z\cos^2\theta) \\
&- \frac{2}{(M_1-M_2)^2(-1+\mathrm{Pr\,Sc\ Sr\ Du})}\mathrm{Br}\,\mathrm{e}^{(y/\sqrt{2})(M_1-M_2)}
\end{aligned}$$

$$\times C_1C_4(M_1M_2 - 2z\cos^2\theta) + \frac{2}{(M_1+M_2)^2(-1+\mathrm{Pr\,Sc\,Sr\,Du})}$$
$$\times \mathrm{Br}\,\mathrm{e}^{(y/\sqrt{2})(M_1+M_2)}C_1C_3(M_1M_2 + 2z\cos^2\theta)$$
$$+ \frac{2}{(M_1+M_2)^2(-1+\mathrm{Pr\,Sc\,Sr\,Du})}\mathrm{Br}\,\mathrm{e}^{-(y/\sqrt{2})(M_1+M_2)}$$
$$\times C_2C_4(M_1M_2 + 2z\cos^2\theta)$$
$$+ \frac{1}{4(1+M_3)(-1+\mathrm{Pr\,Sc\,Sr\,Du})}\mathrm{Br}\,\mathrm{e}^{\sqrt{2}M_2y}$$
$$\times C_3^2(2 + 2M_3 - 2z\eta\cos^2\theta)$$
$$+ \frac{1}{4(-1+M_3)(-1+\mathrm{Pr\,Sc\,Sr\,Du})}\mathrm{Br}\,\mathrm{e}^{\sqrt{2}M_1y}$$
$$\times C_1^2(-2 + 2M_3 + 2z\eta\cos^2\theta), \tag{17}$$

where the constants C_5 and C_6 have the involvement of the Biot numbers Bi_1 and Bi_2. Substituting eq. (17) into eq. (8) we get the closed form solution of $\varphi(y)$ as follows:

$$\begin{aligned}
\varphi(y) \;=\; & C_7 + yC_8 + \frac{\mathrm{Br\,Sc\,Sr}\,zy^2(C_1C_2 + C_3C_4)\cos^2\theta}{-1+\mathrm{Pr\,Sc\,Sr\,Du}} \\
& -\frac{\mathrm{Br}\,\mathrm{e}^{\sqrt{2}M_2y}\mathrm{Sc\,Sr}\,C_3^2(2 + 2M_3 - 2z\eta\cos^2\theta)}{4(1+M_3)(-1+\mathrm{Pr\,Sc\,Sr\,Du})} \\
& +(\mathrm{Br}\,\mathrm{e}^{-\sqrt{2}M_1y}\mathrm{Sc\,Sr}(\mathrm{e}^{2\sqrt{2}M_1y}C_1^2 - 3\mathrm{e}^{2\sqrt{2}M_1y}M_3C_1^2 - 4\mathrm{e}^{2\sqrt{2}M_1y}z\eta C_1^2 \\
& +6\mathrm{e}^{2\sqrt{2}M_1y}M_3z\eta C_1^2 \\
& +6\mathrm{e}^{2\sqrt{2}M_1y}z^2\eta^2C_1^2 + C_2^2 - 3M_3C_2^2 - 4z\eta C_2^2 + 6M_3z\eta C_2^2 \\
& +6z^2\eta^2C_2^2 - 8\mathrm{e}^{(y/\sqrt{2})(3M_1+M_2)} \\
& \times M_1M_2M_3\eta C_1C_3 + 8\mathrm{e}^{(y/\sqrt{2})(3M_1+M_2)}M_3z\eta C_1C_3 \\
& +8\mathrm{e}^{(y/\sqrt{2})(3M_1+M_2)}M_1M_2M_3z\eta^2C_1C_3 \\
& +8\mathrm{e}^{(y/\sqrt{2})(M_1+M_2)}M_1M_2M_3\eta C_2C_3 + 8\mathrm{e}^{(y/\sqrt{2})(M_1+M_2)}M_3z\eta C_2C_3 \\
& -8\mathrm{e}^{(y/\sqrt{2})(M_1+M_2)} \\
& \times M_1M_2M_3z\eta^2C_2C_3 + 8\mathrm{e}^{(y/\sqrt{2})(3M_1-M_2)}M_1M_2M_3\eta C_1C_4 \\
& +8\mathrm{e}^{(y/\sqrt{2})(3M_1-M_2)}M_3z\eta C_1C_4 \\
& -8\mathrm{e}^{(y/\sqrt{2})(3M_1-M_2)}M_1M_2M_3z\eta^2C_1C_4 \\
& -8\mathrm{e}^{(y/\sqrt{2})(M_1-M_2)}M_1M_2M_3\eta C_2C_4 + 8\mathrm{e}^{(y/\sqrt{2})(M_1-M_2)}M_3z\eta C_2C_4 \\
& +8\mathrm{e}^{(y/\sqrt{2})(M_1-M_2)}M_1M_2M_3z\eta^2C_2C_4 - \mathrm{e}^{\sqrt{2}(M_1-M_2)y}C_4^2 \\
& -3\mathrm{e}^{\sqrt{2}(M_1-M_2)y}M_3C_4^2 \\
& +4\mathrm{e}^{\sqrt{2}(M_1-M_2)y}z\eta C_4^2 + 6\mathrm{e}^{\sqrt{2}(M_1-M_2)y}M_3z\eta C_4^2 \\
& -6\mathrm{e}^{\sqrt{2}(M_1-M_2)y}z^2\eta^2C_4^2 + 2z\eta(\mathrm{e}^{2\sqrt{2}M_1y} \\
& \times(-2 + 3M_3 + 4z\eta)C_1^2 + (-2 + 3M_3 + 4z\eta)C_2^2 \\
& +4\mathrm{e}^{(y/\sqrt{2})(3M_1+M_2)}M_3(1 \\
& +M_1M_2\eta)C_1C_3 - 4\mathrm{e}^{(y/\sqrt{2})(M_1+M_2)}M_3(1 + M_1M_2\eta)C_2C_3
\end{aligned}$$

$$
\begin{aligned}
&-4e^{(y/\sqrt{2})(3M_1-M_2)}M_3(-1+M_1M_2\eta)\\
&\times C_1C_4+4e^{(y/\sqrt{2})(M_1-M_2)}M_3(1+M_1M_2\eta)C_2C_4\\
&+e^{\sqrt{2}(M_1-M_2)y}(2+3M_3-4z\eta)C_4^2)\cos 2\theta\\
&+2z^2\eta^2(e^{2\sqrt{2}M_1y}C_1^2+C_2^2-e^{\sqrt{2}(M_1-M_2)y}C_4^2)\cos 4\theta))\\
&/(4(M_1^2-M_2^2)(-1+\mathrm{Pr\,Sc\,Sr\,Du})\eta(-1+4z\eta\cos^2\theta)), \qquad (18)
\end{aligned}
$$

where the constants appearing in the solutions are given in Appendix B.

3. Graphical results and discussion

3.1 *Pumping characteristics*

Figures 2–13 examine the effects of various pertinent flow parameters on the longitudinal pressure gradient $\mathrm{d}p/\mathrm{d}x$ and pressure rise per wavelength Δp_λ. Mathematical form of the pressure gradient is given in eq. (16). Note that eq. (14) involves the integration of $\mathrm{d}p/\mathrm{d}x$. The integral in eq. (14) is not solvable analytically. Hence *Mathematica* has been used for its computation.

Effect of couple-stress parameter η on pressure gradient $\mathrm{d}p/\mathrm{d}x$ against x is plotted in figure 2. It is realized that $\mathrm{d}p/\mathrm{d}x$ increases at the centre of the channel while it decreases near the boundary walls. It is also interesting to note from figure 2 that resistance or assistance from $\mathrm{d}p/\mathrm{d}x$ for a non-Newtonian fluid ($\eta \neq 0$) is higher than the Newtonian fluid ($\eta \to 0$). Figure 3 indicates that $\mathrm{d}p/\mathrm{d}x$ decreases at the centre of the channel and it increases near the boundary walls with an increase of Hall parameter m. Figure 4 elucidates the decreasing behaviour of $\mathrm{d}p/\mathrm{d}x$ at the centre of the channel and it has increasing behaviour near the channel walls with the increasing values of inclination angle θ for magnetic field.

Figures 5–7 illustrate the variation of pressure rise per wavelength Δp_λ vs. average flux σ. From figure 5 we observe that in peristaltic pumping region ($\Delta p_\lambda > 0, \sigma > 0$) the pressure rise increases while it decreases in the co-pumping region ($\Delta p_\lambda < 0, \sigma > 0$) with an increase in the couple-stress parameter η. It means that the peristaltic pumping

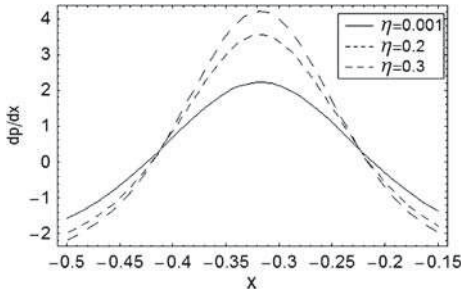

Figure 2. Plot of pressure gradient $\mathrm{d}p/\mathrm{d}x$ for various values of η when $a = 0.6$, $b = 0.7$, $d = 1.5$, $R = 0.5$, $\phi = \pi/4$, $\sigma = 1$, $\alpha = \pi/3$, $m = 0.03$, $\mathrm{Fr} = 1.2$, $\theta = \pi/3$ and $M = 4$.

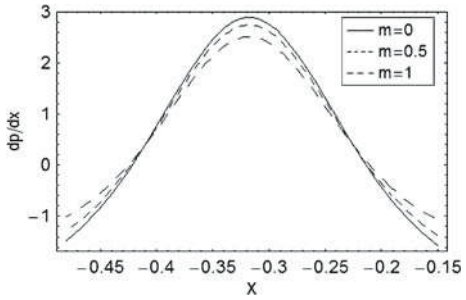

Figure 3. Plot of pressure gradient $\mathrm{d}p/\mathrm{d}x$ for various values of m when $a = 0.6$, $b = 0.7$, $d = 1.5$, $R = 0.5$, $\phi = \pi/4$, $\sigma = 1$, $\alpha = \pi/3$, Fr $= 1.2$, $\theta = \pi/3$, $\eta = 0.1$ and $M = 4$.

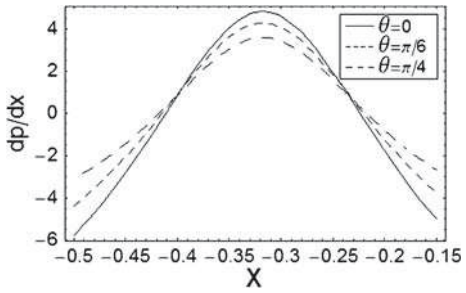

Figure 4. Plot of pressure gradient $\mathrm{d}p/\mathrm{d}x$ for various values of θ when $a = 0.6$, $b = 0.7$, $d = 1.5$, $R = 0.5$, Fr $= 1.2$, $\sigma = 1$, $\alpha = \pi/3$, $\eta = 0.1$, $\phi = \pi/4$, $m = 0.03$ and $M = 4$.

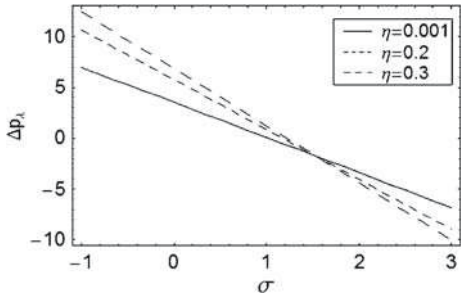

Figure 5. Plot of pressure rise ΔP_λ for various values of η when $a = 0.7$, $b = 1.2$, $d = 2$, $R = 0.5$, Fr $= 1.2$, $\alpha = \pi/3$, $\phi = \pi/4$, $m = 0.03$, $M = 4$ and $\theta = \pi/3$.

for the non-Newtonian fluid ($\eta \neq 0$) is greater than that for the Newtonian fluid ($\eta \to 0$). Figure 6 reveals that the pressure rise decreases in the retrograde ($\Delta p_\lambda > 0, \sigma < 0$) region and it increases in the co-pumping region ($\Delta p_\lambda < 0, \sigma > 0$) as the Hall parameter m increases. Figure 7 elucidates that the pressure rise decreases in the peristaltic pumping region ($\Delta p_\lambda > 0, \sigma > 0$) when there is an increase in the angle of inclination θ of the magnetic field and it increases in the co-pumping region ($\Delta p_\lambda < 0, \sigma > 0$).

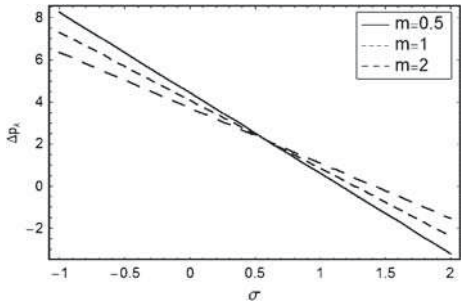

Figure 6. Plot of pressure rise ΔP_λ for various values of m when $a = 0.7$, $b = 1.2$, $d = 2$, $R = 0.5$, Fr$= 1.2$, $\alpha = \pi/3$, $\phi = \pi/4$, $\eta = 0.1$, $M = 4$ and $\theta = \pi/3$.

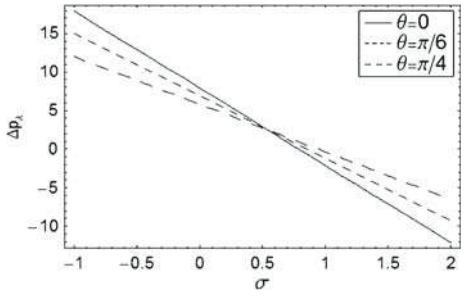

Figure 7. Plot of pressure rise ΔP_λ for various values of θ when $a = 0.7$, $b = 1.2$, $d = 2$, $R = 0.5$, Fr$= 1.2$, $\alpha = \pi/3$, $\phi = \pi/4$, $m = 0.03$, $\eta = 0.1$ and $M = 4$.

3.2 *Velocity behaviour*

In this subsection we discuss the effect of various physical parameters on the velocity profile $u(y)$. Mathematical form of the velocity is given in eq. (15). Figure 8 shows that the longitudinal velocity profile $u(y)$ decreases when couple-stress parameter η increases. It is also interesting to note that for non-Newtonian fluid ($\eta \neq 0$) the longitudinal velocity

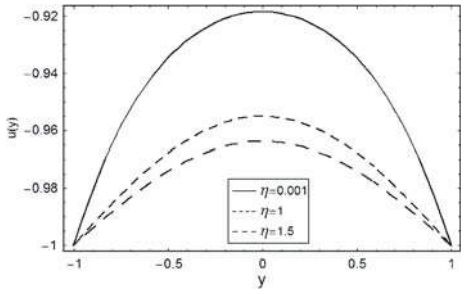

Figure 8. Plot of velocity field $u(y)$ for various values of η when $a = 0.6$, $b = 0.7$, $d = 1.5$, $R = 0.5$, Fr $= 1.2$, $\sigma = 1$, $\alpha = \pi/3$, $M = 4$, $\phi = \pi/4$, $m = 0.03$, $\theta = \pi/3$, $x = -0.5$ and $\mathrm{d}p/\mathrm{d}x = 1$.

profile $u(y)$ is lesser than that of Newtonian fluid ($\eta \to 0$). As couple-stress parameter depends on the couple-stress viscosity and this couple-stress viscosity acts as a retarding agent which makes the fluid more dense resulting in a decrease in the velocity of the fluid. Figure 9 gives the information that for subcritical flow (Fr < 1) the velocity profile $u(y)$ has greater effect than that of critical (Fr $= 1$) and supercritical

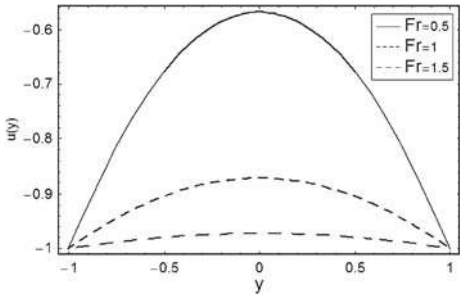

Figure 9. Plot of velocity field $u(y)$ for various values of Fr when $a = 0.6$, $b = 0.7$, $d = 1.5$, $R = 0.5$, $\eta = 0.1$, $\sigma = 1$, $\alpha = \pi/3$, $M = 4$, $\phi = \pi/4$, $m = 0.03$, $\theta = \pi/3$, $x = -0.5$ and $\mathrm{d}p/\mathrm{d}x = 1$.

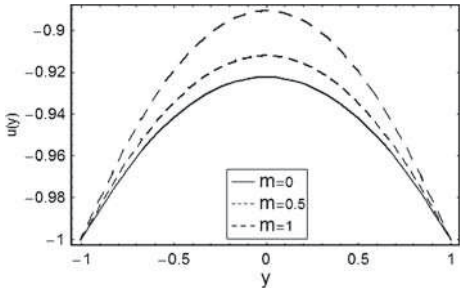

Figure 10. Plot of velocity field $u(y)$ for various values of m when $a = 0.6$, $b = 0.7$, $d = 1.5$, $R = 0.5$, $\eta = 0.1$, $\sigma = 1$, $\alpha = \pi/3$, Fr $= 1.2$, $\phi = \pi/4$, $M = 4$, $\theta = \pi/3$, $\mathrm{d}p/\mathrm{d}x = 1$ and $x = -0.5$.

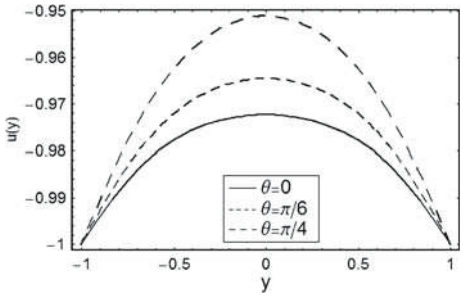

Figure 11. Plot of velocity field $u(y)$ for various values of θ when $a = 0.6$, $b = 0.7$, $d = 1.5$, $R = 0.5$, $\eta = 0.1$, $\sigma = 1$, $\alpha = \pi/3$, Fr $= 1.2$, $\phi = \pi/4$, $m = 0.03$, $M = 4$, $\mathrm{d}p/\mathrm{d}x = 1$ and $x = -0.5$.

(Fr $>$ 1) flow. The velocity profile $u(y)$ decreases with an increase of Froude number Fr. Figure 10 demonstrates that the increase the velocity profile $u(y)$ increases as Hall parameter m increases. Figure 11 shows that with an increase in inclination angle θ of the magnetic field ($\theta \neq 0$), the longitudinal velocity $u(y)$ has greater value in comparison to the case when $\theta = 0$.

3.3 *Temperature profile*

Figures 12–20 demonstrate the variation of temperature profile $\gamma(y)$ for embedded physical parameters. From figure 12 it is clear that as couple-stress parameter η increases, the temperature profile $\gamma(y)$ decreases. In fact, the average kinetic energy decreases due to the decrease in velocity of the fluid and hence temperature decays. Figure 13 depicts that with an increase of inclination angle θ of the magnetic field, the temperature profile $\gamma(y)$ increases. Similar observation is noticed for Hall parameter m (see figure 14). It is found from figure 15 that the temperature profile $\gamma(y)$ has greater effects for supercritical

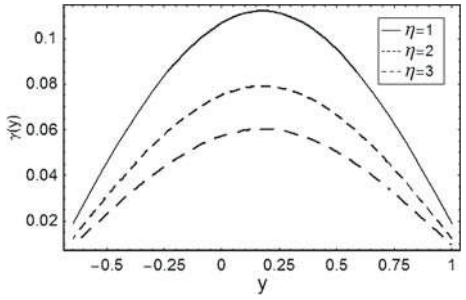

Figure 12. Plot of temperature profile $\gamma(y)$ for various values of η when $a = 0.5$, $b = 0.5$, $d = 1$, $R = 0.2$, $M = 4$, $\sigma = 1$, $\alpha = \pi/3$, Fr $= 1.2$, $\phi = \pi/4$, $m = 0.03$, $\theta = \pi/3$, $\mathrm{d}p/\mathrm{d}x = 2$, $x = -0.5$, Du $= 0.1$, $\mathrm{Bi}_1 = 10$, $\mathrm{Bi}_2 = 10$, Sc $= 0.5$, Sr $= 0.6$, Pr $= 2$ and Br $= 2$.

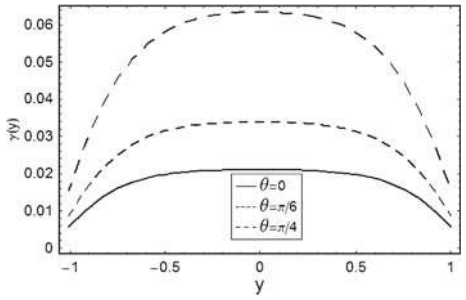

Figure 13. Plot of temperature profile $\gamma(y)$ for various values of θ when $a = 0.6$, $b = 0.7$, $d = 1.5$, $R = 0.2$, $M = 4$, $\sigma = 1$, $\alpha = \pi/3$, Fr $= 1.2$, $\phi = \pi/4$, $m = 0.03$, $\eta = 0.1$, $\mathrm{d}p/\mathrm{d}x = 2$, $x = -0.5$, Du $= 0.1$, $\mathrm{Bi}_1 = 10$, $\mathrm{Bi}_2 = 10$, Sc $= 0.5$, Sr $= 0.6$, Pr $= 2$ and Br $= 2$.

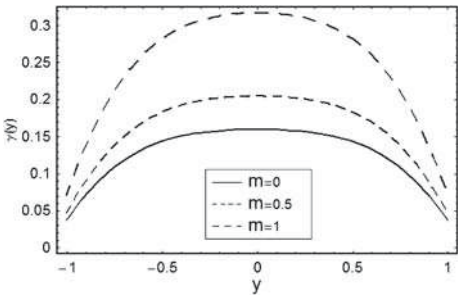

Figure 14. Plot of temperature profile $\gamma(y)$ for various values of m when $a = 0.6$, $b = 0.7$, $d = 1.5$, $R = 0.2$, $M = 4$, $\sigma = 1$, $\alpha = \pi/3$, Fr $= 1.2$, $\phi = \pi/4$, $\eta = 0.1$, $\theta = \pi/3$, $\mathrm{d}p/\mathrm{d}x = 2$, $x = -0.5$, Du $= 0.1$, $\mathrm{Bi}_1 = 10$, $\mathrm{Bi}_2 = 10$, Sc $= 0.5$, Sr $= 0.6$, Pr $= 2$ and Br $= 2$.

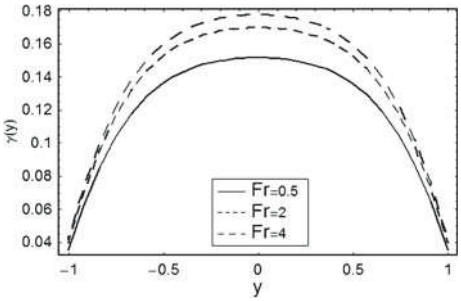

Figure 15. Plot of temperature profile $\gamma(y)$ for various values of Fr when $a = 0.6$, $b = 0.7$, $d = 1.5$, $R = 0.2$, $M = 4$, $\sigma = 1$, $\alpha = \pi/3$, $\eta = 0.1$, $\phi = \pi/4$, $m = 0.03$, $\theta = \pi/3$, $\mathrm{d}p/\mathrm{d}x = 2$, $x = -0.5$, Du $= 0.1$, $\mathrm{Bi}_1 = 10$, $\mathrm{Bi}_2 = 10$, Sc $= 0.5$, Sr $= 0.6$, Pr $= 2$ and Br $= 2$.

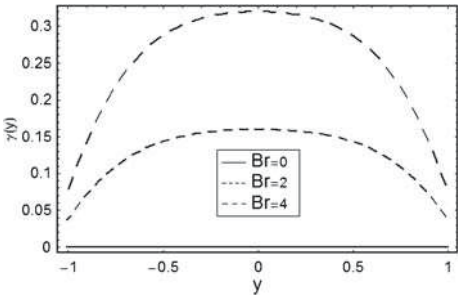

Figure 16. Plot of temperature profile $\gamma(y)$ for various values of Br when $a = 0.6$, $b = 0.7$, $d = 1.5$, $R = 0.2$, $M = 4$, $\sigma = 1$, $\alpha = \pi/3$, Fr $= 1.2$, $\phi = \pi/4$, $m = 0.03$, $\theta = \pi/3$, $\mathrm{d}p/\mathrm{d}x = 2$, $x = -0.5$, Du $= 0.1$, $\mathrm{Bi}_1 = 10$, $\mathrm{Bi}_2 = 10$, Sc $= 0.5$, Sr $= 0.6$, Pr $= 2$ and $\eta = 0.1$.

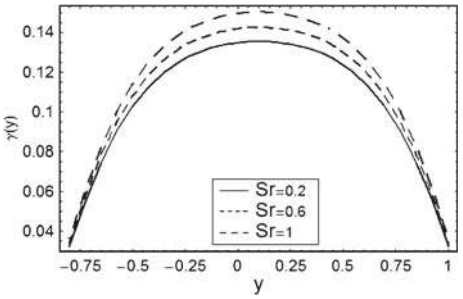

Figure 17. Plot of temperature profile $\gamma(y)$ for various values of Sr when $a = 0.6$, $b = 0.7$, $d = 1.5$, $R = 0.2$, $M = 4$, $\sigma = 1$, $\alpha = \pi/3$, Fr $= 1.2$, $\phi = \pi/4$, $m = 0.03$, $\theta = \pi/3$, $\mathrm{d}p/\mathrm{d}x = 2$, $x = -0.5$, Du $= 0.1$, $\mathrm{Bi}_1 = 10$, $\mathrm{Bi}_2 = 10$, Sc $= 0.5$, Br $= 2$, Pr $= 2$ and $\eta = 0.1$.

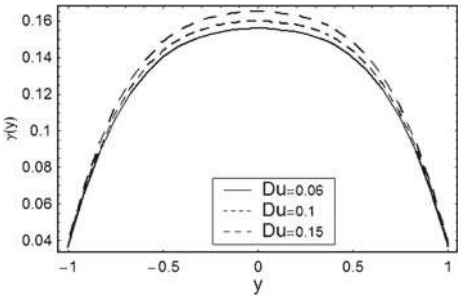

Figure 18. Plot of temperature profile $\gamma(y)$ for various values of Du when $a = 0.6$, $b = 0.7$, $d = 1.5$, $R = 0.2$, $M = 4$, $\sigma = 1$, $\alpha = \pi/3$, Fr $= 1.2$, $\phi = \pi/4$, $m = 0.03$, $\theta = \pi/3$, $\mathrm{d}p/\mathrm{d}x = 2$, $x = -0.5$, Br $= 2$, $\mathrm{Bi}_1 = 10$, $\mathrm{Bi}_2 = 10$, Sc $= 0.5$, Sr $= 0.6$, Pr $= 2$ and $\eta = 0.1$.

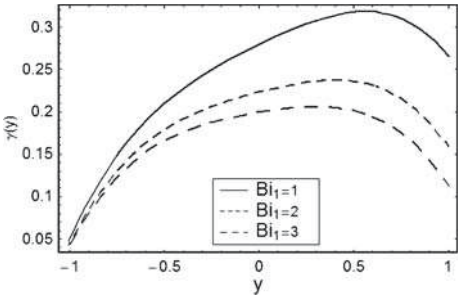

Figure 19. Plot of temperature profile $\gamma(y)$ for various values of Bi_1 when $a = 0.6$, $b = 0.7$, $d = 1.5$, $R = 0.2$, $M = 4$, $\sigma = 1$, $\alpha = \pi/3$, Fr $= 1.2$, $\phi = \pi/4$, $m = 0.03$, $\theta = \pi/3$, $\mathrm{d}p/\mathrm{d}x = 2$, $x = -0.5$, Br $= 2$, Du $= 0.1$, $\mathrm{Bi}_2 = 10$, Sc $= 0.5$, Sr $= 0.6$, Pr $= 2$ and $\eta = 0.1$.

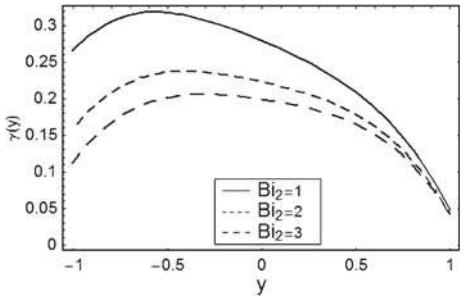

Figure 20. Plot of temperature profile $\gamma(y)$ for various values of Bi_2 when $a = 0.6$, $b = 0.7$, $d = 1.5$, $R = 0.2$, $M = 4$, $\sigma = 1$, $\alpha = \pi/3$, Fr $= 1.2$, $\phi = \pi/4$, $m = 0.03$, $\theta = \pi/3$, $\mathrm{d}p/\mathrm{d}x = 2$, $x = -0.5$, Br $= 2$, Du $= 0.1$, $\mathrm{Bi}_1 = 10$, Sc $= 0.5$, Sr $= 0.6$, Pr $= 2$.

flow (Fr $>$ 1) and critical flow (Fr $=$ 1) than subcritical flow (Fr $<$ 1). The temperature profile $\gamma(y)$ increases with an increase of Froude number Fr. In figure 16 we see the effect of Br on $\gamma(y)$. Brinkman number Br $= 0$ means that the effect of viscous dissipation is not considered and when Brinkman number Br $\neq 0$ the effects of viscous dissipation are taken into account and then the temperature profile $\gamma(y)$ increases. It is noticed that temperature profile $\gamma(y)$ increases with an increase in the value Sr as shown in figure 17. It is also noticed from figure 18 that the temperature profile $\gamma(y)$ has an increasing behaviour for large values of Dufour number Du. Figure 19 elucidates that with an increase of Bi_1 the temperature profile $\gamma(y)$ decreases near the upper wall while it has no significant effect near the lower wall. On the other hand, with an increase in Bi_2 the temperature profile decreases near the lower wall and it has no significant effect near the upper wall (see figure 20). Also we have considered Biot numbers much larger than 0.1 because of the consideration of non-uniform temperature fields within the fluid.

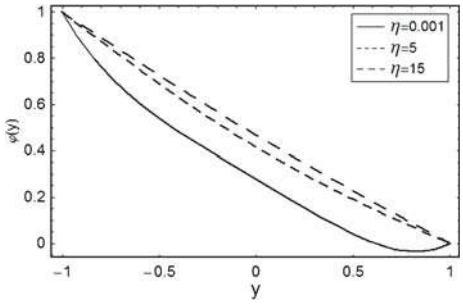

Figure 21. Plot of concentration profile $\varphi(y)$ for various values of η when $a = 0.6$, $b = 0.7$, $d = 1.5$, $R = 0.2$, $M = 2$, $\sigma = 1$, $\alpha = \pi/3$, Fr $= 1.2$, $\phi = \pi/4$, $m = 0.03$, $\theta = \pi/3$, $\mathrm{d}p/\mathrm{d}x = 2$, $x = -0.5$, Br $= 2$, Sr $= 0.6$, Du $= 0.1$, Pr $= 4$ and Sc $= 1$.

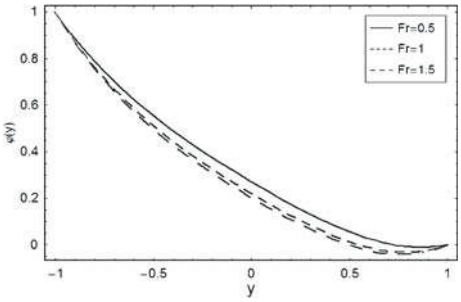

Figure 22. Plot of concentration profile $\varphi(y)$ for various values of Fr when $a = 0.6$, $b = 0.7$, $d = 1.5$, $R = 0.2$, $M = 2$, $\sigma = 1$, $\alpha = \pi/3$, $\eta = 0.1$, $\phi = \pi/3$, $m = 0.03$, $\theta = \pi/3$, $\mathrm{d}p/\mathrm{d}x = 2$, $x = -0.5$, Br $= 2$, Sr $= 0.6$, Du $= 0.1$, Pr $= 4$ and Sc $= 1$.

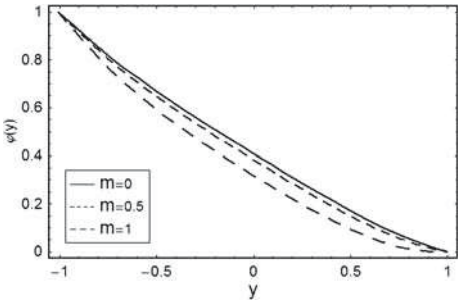

Figure 23. Plot of concentration profile $\varphi(y)$ for various values of m when $a = 0.6$, $b = 0.7$, $d = 1.5$, $R = 0.2$, $M = 2$, $\sigma = 1$, $\alpha = \pi/3$, Fr $= 1.2$, $\phi = \pi/3$, $\eta = 0.1$, $\theta = \pi/3$, $\mathrm{d}p/\mathrm{d}x = 2$, $x = -0.5$, Br $= 2$, Sr $= 0.6$, Du $= 0.1$, Pr $= 4$ and Sc $= 1$.

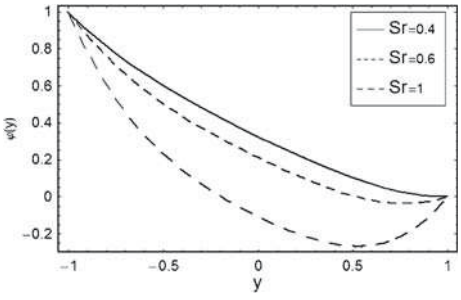

Figure 24. Plot of concentration profile $\varphi(y)$ for various values of Sr when $a = 0.6$, $b = 0.7$, $d = 1.5$, $R = 0.2$, $M = 2$, $\sigma = 1$, $\alpha = \pi/3$, Fr $= 1.2$, $\phi = \pi/3$, $m = 0.03$, $\theta = \pi/3$, $\mathrm{d}p/\mathrm{d}x = 2$, $x = -0.5$, Br $= 2$, $\eta = 0.1$, Du $= 0.1$, Pr $= 4$ and Sc $= 1$.

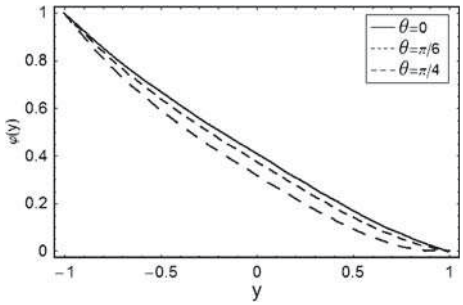

Figure 25. Plot of concentration profile $\varphi(y)$ for various values of θ when $a = 0.6$, $b = 0.7$, $d = 1.5$, $R = 0.2$, $M = 2$, $\sigma = 1$, $\alpha = \pi/3$, Fr $= 1.2$, $\phi = \pi/3$, $m = 0.03$, $\eta = 0.1$, $\mathrm{d}p/\mathrm{d}x = 2$, $x = -0.5$, Br $= 2$, Sr $= 0.6$, Du $= 0.1$, Pr $= 4$ and Sc $= 1$.

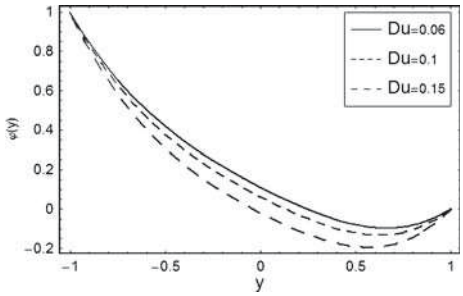

Figure 26. Plot of concentration profile $\varphi(y)$ for various values of Du when $a = 0.6$, $b = 0.7$, $d = 1.5$, $R = 0.2$, $M = 2$, $\sigma = 1$, $\alpha = \pi/3$, Fr $= 1.2$, $\phi = \pi/3$, $m = 0.03$, $\theta = \pi/3$, $\mathrm{d}p/\mathrm{d}x = 2$, $x = -0.5$, Br $= 2$, $\eta = 0.1$, Sr $= 0.6$, Pr $= 4$ and Sc $= 1$.

3.4 *Concentration profile*

The purpose of this subsection is to see the salient features of concentration profile $\varphi(y)$ for different values of the involved parameters. Figure 21 shows that $\varphi(y)$ increases when η increases. In non-Newtonian fluid ($\eta \neq 0$), the concentration profile $\varphi(y)$ has greater effect than that of Newtonian fluids ($\eta \to 0$). Figure 22 displays that for subcritical flow (Fr < 1) the concentration profile $\varphi(y)$ is greater than the critical flow (Fr $= 1$) and supercritical flow (Fr > 1). It means that as the Froude number Fr increases, the concentration profile $\varphi(y)$ decreases. It is revealed from figure 23 that the concentration profile $\varphi(y)$ decreases by an increase in Hall parameter m. Figure 24 shows that for larger Sr the concentration profile $\varphi(y)$ decreases. Figures 25 and 26 depict that concentration profile $\varphi(y)$ decreases when θ and Dufour number Du increase (figures 27, 28 and 29).

3.5 *Trapping*

Effect of Froude number Fr on trapping is illustrated in figure 27. It is observed that the size of the trapped bolus decreases when Fr increases and it disappears for (supercritical

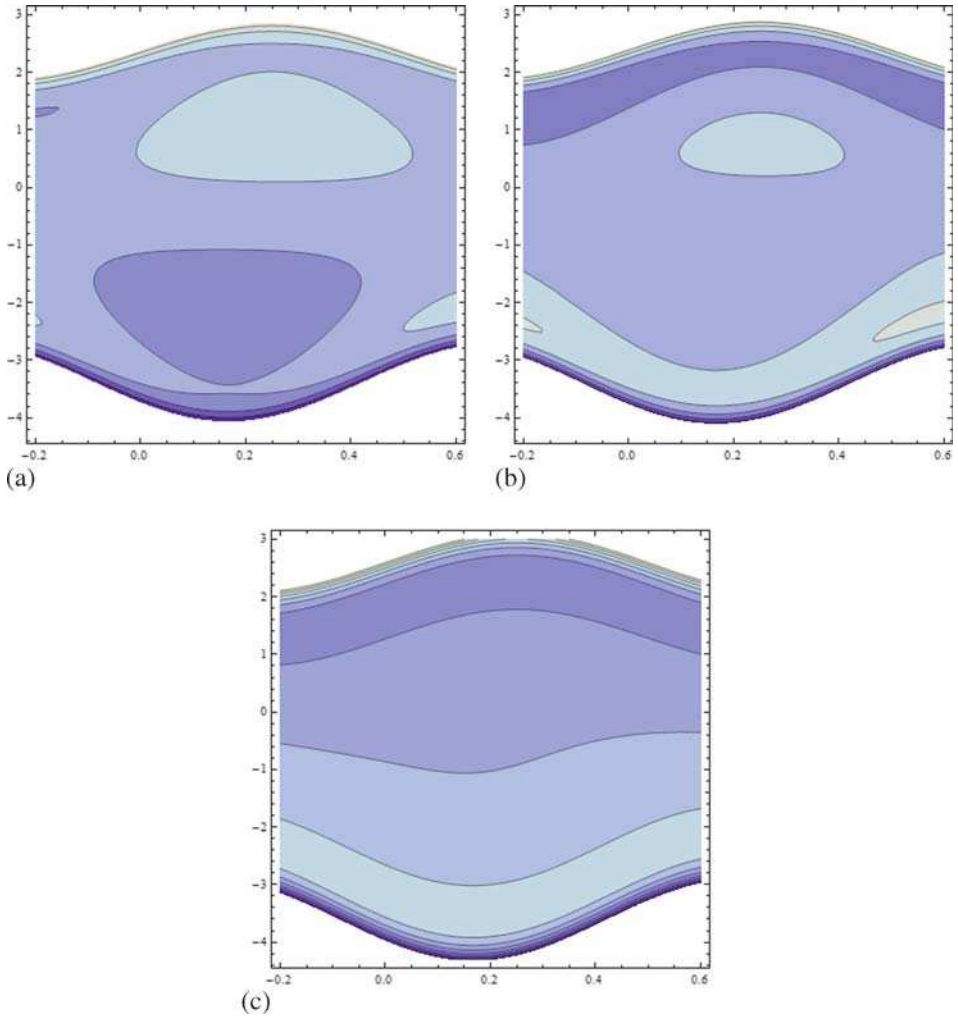

Figure 27. Streamlines for $a = 0.5$, $b = 0.7$, $R = 10$, $d = 2$, $\phi = \pi/6$, $\sigma = 1$, $\alpha = \pi/3$, $\mathrm{d}p/\mathrm{d}x = 2$, $m = 0.03$, $\eta = 0.1$, $\theta = \pi/3$, $M = 3$ when (**a**) Fr = 1, (**b**) Fr = 1.5, (**c**) Fr = 2.

flow Fr>1) Fr = 2 (see panel (c)). It is concluded from figure 28 that when couple-stress parameter η increases, the bolus decreases in size. Figure 29 shows that by increasing the values of m the trapping bolus reduces in size.

4. Conclusions

The peristaltic flow of couple-stress fluid in an inclined asymmetric channel with convective conditions was discussed. Effect of Soret (thermodiffusion) and Dufour (diffusion-thermo) were also considered. Effect of Hall current was taken into account. The main findings of the present research are mentioned below.

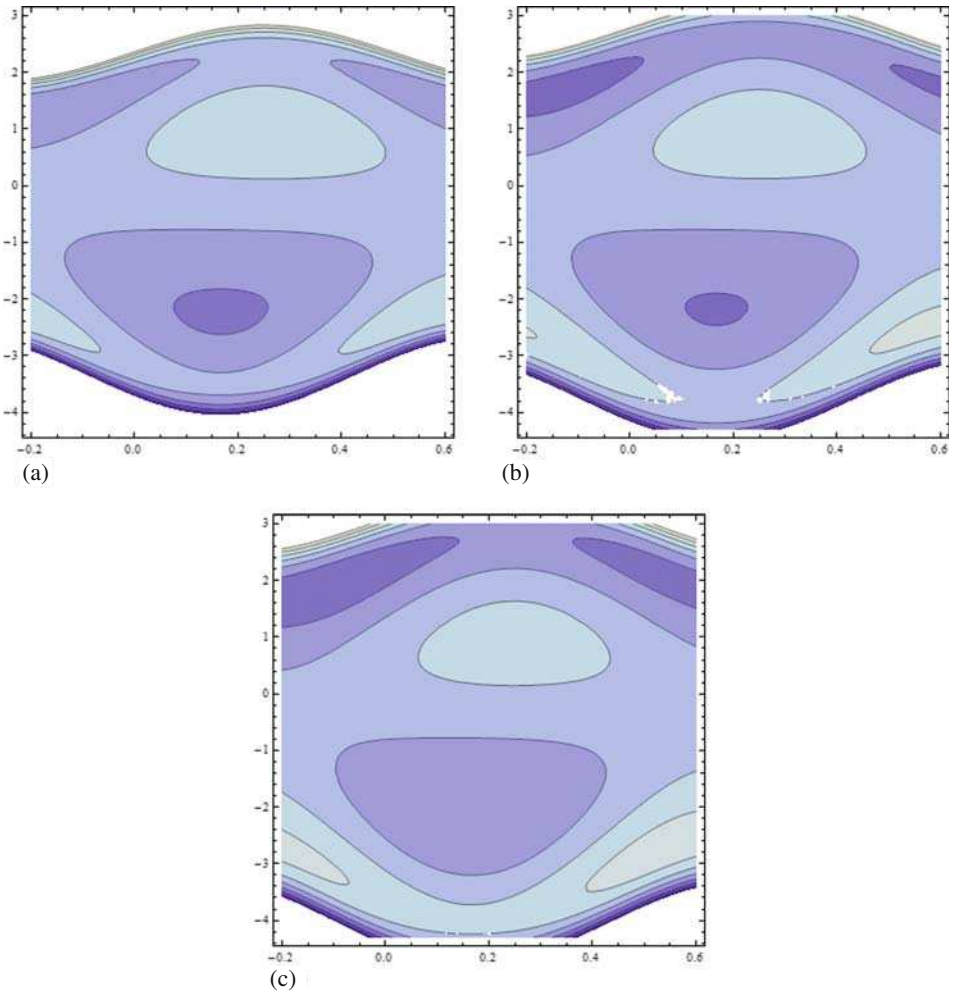

Figure 28. Streamlines for $a = 0.5$, $b = 0.7$, $R = 10$, $d = 2$, $\phi = \pi/6$, $\sigma = 1$, $\alpha = \pi/3$, $\mathrm{d}p/\mathrm{d}x = 2$, $m = 0.03$, Fr $= 1.2$, $\theta = \pi/3$, $M = 3$ when (**a**) $\eta = 1$, (**b**) $\eta = 1.5$, (**c**) $\eta = 2$.

(1) Pressure gradient $\mathrm{d}p/\mathrm{d}x$ shows the increasing and decreasing behaviour at the centre of the channel and near the boundary walls respectively when η increases.
(2) For increasing Hall parameter m, the pressure gradient $\mathrm{d}p/\mathrm{d}x$ increases near the boundary walls and decreases at the centre of the channel.
(3) Pressure rise Δp_λ decreases in the retrograde region and increases in the co-pumping region when the Hall parameter m increases. Similar behaviour is observed for inclination angle θ of the magnetic field.
(4) Magnitude of the velocity profile $u(y)$ increases when there is an increase in the inclination angle θ of the magnetic field and Hall parameter m.
(5) Velocity profile $u(y)$ decreases with increasing values of couple-stress parameter η.

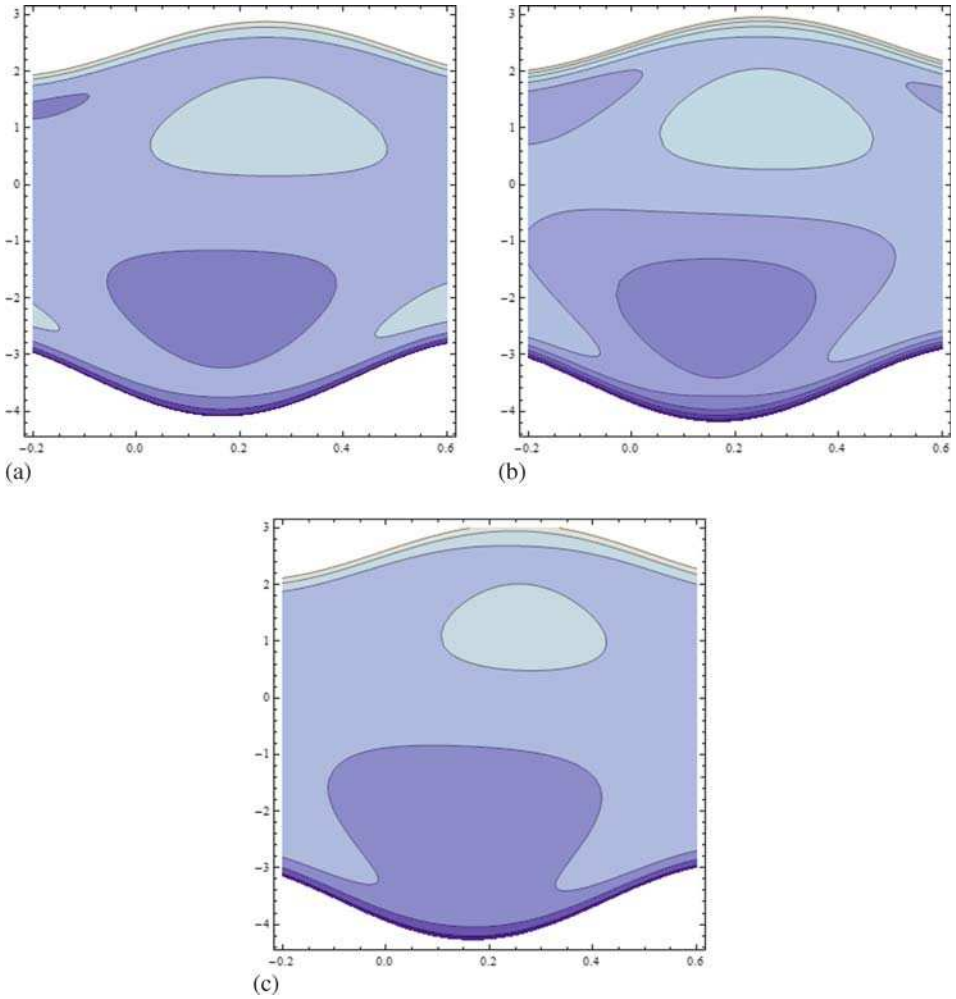

Figure 29. Streamlines for $a = 0.5$, $b = 0.7$, $R = 10$, $d = 2$, $\phi = \pi/6$, $\sigma = 1$, $\alpha = \pi/3$, $\mathrm{d}p/\mathrm{d}x = 2$, $M = 3$, $\eta = 0.1$, $\theta = \pi/3$, Fr $= 1.2$ when (**a**) $m = 0.5$, (**b**) $m = 1$, (**c**) $m = 1.5$.

(6) Temperature profile $\gamma(y)$ increases when Hall parameter m and Froude number Fr are enhanced.
(7) With an increase in the Biot numbers (Bi_1, Bi_2) the temperature profile $\gamma(y)$ decreases.
(8) Concentration profile $\varphi(y)$ is a decreasing function of Fr, m and Du.
(9) The size of the trapping bolus decreases with the increase in Froude number Fr and Hall parameter m while it increases when the angle of inclination of the channel increases.

Acknowledgements

The authors are grateful to the reviewer for the useful suggestions. This paper was funded by the Deanship of Scientific Research (DSR), King Abdulaziz University, Jeddah

under grant no. (8-13/1434HiCi). The authors, therefore, acknowledge with thanks DSR technical and financial support.

Appendix A

The conservation laws for the governing flow problems are as follows:

$$\frac{\partial \bar{U}}{\partial \bar{X}} + \frac{\partial \bar{V}}{\partial \bar{Y}} = 0, \tag{A1}$$

$$\rho\left(\frac{\partial}{\partial \bar{t}} + \bar{U}\frac{\partial}{\partial \bar{X}} + \bar{V}\frac{\partial}{\partial \bar{Y}}\right)\bar{U} = -\frac{\partial \bar{P}}{\partial \bar{X}} + \mu\left(\frac{\partial^2 \bar{U}}{\partial \bar{X}^2} + \frac{\partial^2 \bar{U}}{\partial \bar{Y}^2}\right) - \eta^*\left(\frac{\partial^4 \bar{U}}{\partial \bar{X}^4} + 2\frac{\partial^4 \bar{U}}{\partial \bar{X}^2 \partial \bar{Y}^2} + \frac{\partial^4 \bar{U}}{\partial \bar{Y}^4}\right) - \frac{\sigma^* B_0^2}{1+m^2}\cos\theta\left(\bar{U}\cos\theta - \bar{V}\sin\theta\right) + g\rho\sin\alpha, \tag{A2}$$

$$\rho\left(\frac{\partial}{\partial \bar{t}} + \bar{U}\frac{\partial}{\partial \bar{X}} + \bar{V}\frac{\partial}{\partial \bar{Y}}\right)\bar{V} = -\frac{\partial \bar{P}}{\partial \bar{Y}} + \mu\left(\frac{\partial^2 \bar{V}}{\partial \bar{X}^2} + \frac{\partial^2 \bar{V}}{\partial \bar{Y}^2}\right) - \eta^*\left(\frac{\partial^4 \bar{V}}{\partial \bar{X}^4} + 2\frac{\partial^4 \bar{V}}{\partial \bar{X}^2 \partial \bar{Y}^2} + \frac{\partial^4 \bar{V}}{\partial \bar{Y}^4}\right) + \frac{\sigma^* B_0^2}{1+m^2}\sin\theta\left(\bar{U}\cos\theta - \bar{V}\sin\theta\right) - g\rho\cos\alpha, \tag{A3}$$

$$\rho\xi\left(\frac{\partial}{\partial \bar{t}} + \bar{U}\frac{\partial}{\partial \bar{X}} + \bar{V}\frac{\partial}{\partial \bar{Y}}\right)T = \kappa\left(\frac{\partial^2 T}{\partial \bar{X}^2} + \frac{\partial^2 T}{\partial \bar{Y}^2}\right) + \mu\left[2\left(\frac{\partial \bar{U}}{\partial \bar{X}}\right)^2 + 2\left(\frac{\partial \bar{V}}{\partial \bar{Y}}\right)^2 + \left(\frac{\partial \bar{U}}{\partial \bar{Y}} + \frac{\partial \bar{V}}{\partial \bar{X}}\right)^2\right] + \eta^*\left[\left(\frac{\partial^2 \bar{V}}{\partial \bar{X}^2} + \frac{\partial^2 \bar{V}}{\partial \bar{Y}^2}\right)^2 + \left(\frac{\partial^2 \bar{U}}{\partial \bar{X}^2} + \frac{\partial^2 \bar{U}}{\partial \bar{Y}^2}\right)^2\right] + \frac{\rho D K_T}{c_s}\left(\frac{\partial^2 C}{\partial \bar{X}^2} + \frac{\partial^2 C}{\partial \bar{Y}^2}\right), \tag{A4}$$

$$\left(\frac{\partial}{\partial \bar{t}} + \bar{U}\frac{\partial}{\partial \bar{X}} + \bar{V}\frac{\partial}{\partial \bar{Y}}\right)C = D\left(\frac{\partial^2 C}{\partial \bar{X}^2} + \frac{\partial^2 C}{\partial \bar{Y}^2}\right) + \frac{DK_T}{T_m}\left(\frac{\partial^2 T}{\partial \bar{X}^2} + \frac{\partial^2 T}{\partial \bar{Y}^2}\right). \tag{A5}$$

The boundary conditions and geometry of the channel walls are given by

$$\bar{U} = 0, \quad \kappa\frac{\partial T}{\partial \bar{Y}} = -\eta_1\left(T - T_{\mathrm{a}}\right), \quad C = C_0,$$

at

$$\bar{Y} = \bar{H}_1(\bar{X}, \bar{t}) = d_1 + a_1 \sin\left[\frac{2\pi}{\lambda}(\bar{X} - c\bar{t})\right], \tag{A6}$$

$$\bar{U} = 0, \quad \kappa \frac{\partial T}{\partial \bar{Y}} = -\eta_2 (T_a - T), \; C = C_1,$$

at

$$\bar{Y} = \bar{H}_2(\bar{X}, \bar{t}) = -d_2 - a_2 \sin\left[\frac{2\pi}{\lambda}(\bar{X} - c\bar{t}) + \phi\right], \tag{A7}$$

where $\bar{P}$, C, T, k, ξ, T_m, D, ρ and K_T are respectively the pressure, concentration, temperature, thermal conductivity, specific heat at constant pressure, mean temperature of the medium, coefficient of mass diffusivity, fluid density and thermal-diffusion ratio. Further c_s is the concentration susceptibility, η^* is the couple-stress fluid parameter and α is the inclination of the channel. Here η_1 and η_2 are the heat transfer coefficients at the upper and lower walls respectively, T is the temperature of the fluid, T_a is the ambient temperature, C_0 and C_1 are the concentration fields of the upper and lower walls respectively, d_1 and d_2 are the distances of the upper and lower walls of the channel from the centerline ($\bar{Y} = 0$), a_i ($i = 1, 2$) are the wave amplitudes at the upper and lower walls, λ is the wavelength, $\bar{t}$ is the time and ϕ is the phase difference varying in the range $0 \le \phi \le \pi$. Here $\phi = 0$ corresponds to symmetric channel with waves out of phase and $\phi = \pi$ the waves in phase, $\rho g \sin\alpha$ and $\rho g \cos\alpha$ are the $\bar{X}$ and $\bar{Y}$ components of the body force in view of the inclined channel and $\bar{H}_1$ and $\bar{H}_2$ are the upper and lower walls of the channel. Moreover, a_i and d_i ($i = 1, 2$) satisfy the condition

$$a_1^2 + a_2^2 + 2a_1 a_2 \cos\phi \le (d_1 + d_2)^2. \tag{A8}$$

Using the transformations

$$\bar{x} = \bar{X} - c\bar{t}, \quad \bar{y} = \bar{Y}, \quad \bar{u}(\bar{x}, \bar{y}) = \bar{U}(\bar{X}, \bar{Y}, \bar{t}) - c$$
$$\bar{v}(\bar{x}, \bar{y}) = \bar{V}(\bar{X}, \bar{Y}, \bar{t}), \; \bar{p}(\bar{x}, \bar{y}) = \bar{P}(\bar{X}, \bar{Y}, \bar{t}), \tag{A9}$$

the equations in the wave frame $(\bar{x}, \bar{y})$ are given by

$$\frac{\partial \bar{u}}{\partial \bar{x}} + \frac{\partial \bar{v}}{\partial \bar{y}} = 0, \tag{A10}$$

$$\rho\left(\bar{u}\frac{\partial}{\partial \bar{x}} + \bar{v}\frac{\partial}{\partial \bar{y}}\right)\bar{u} = -\frac{\partial \bar{p}}{\partial \bar{x}} + \mu\left(\frac{\partial^2 \bar{u}}{\partial \bar{x}^2} + \frac{\partial^2 \bar{u}}{\partial \bar{y}^2}\right) - \eta^*\left(\frac{\partial^4 \bar{u}}{\partial \bar{x}^4} + 2\frac{\partial^4 \bar{u}}{\partial \bar{x}^2 \partial \bar{y}^2} + \frac{\partial^4 \bar{u}}{\partial \bar{y}^4}\right)$$
$$- \frac{\sigma^* B_0^2}{1 + m^2}\cos\theta\,[(\bar{u} + c)\cos\theta - \bar{v}\sin\theta] + g\rho\sin\alpha, \tag{A11}$$

$$\rho\left(\bar{u}\frac{\partial}{\partial \bar{x}} + \bar{v}\frac{\partial}{\partial \bar{y}}\right)\bar{v} = -\frac{\partial \bar{p}}{\partial \bar{y}} + \mu\left(\frac{\partial^2 \bar{v}}{\partial \bar{x}^2} + \frac{\partial^2 \bar{v}}{\partial \bar{y}^2}\right) - \eta^*\left(\frac{\partial^4 \bar{v}}{\partial \bar{x}^4} + 2\frac{\partial^4 \bar{v}}{\partial \bar{x}^2 \partial \bar{y}^2} + \frac{\partial^4 \bar{v}}{\partial \bar{y}^4}\right)$$
$$+ \frac{\sigma^* B_0^2}{1 + m^2}\sin\theta\,[(\bar{u} + c)\cos\theta - \bar{v}\sin\theta] - g\rho\cos\alpha, \tag{A12}$$

$$\rho\xi\left(\bar{u}\frac{\partial}{\partial\bar{x}}+\bar{v}\frac{\partial}{\partial\bar{y}}\right)T = \kappa\left(\frac{\partial^2 T}{\partial\bar{x}^2}+\frac{\partial^2 T}{\partial\bar{y}^2}\right) + \mu\left(2\left(\frac{\partial\bar{u}}{\partial\bar{x}}\right)^2+2\left(\frac{\partial\bar{v}}{\partial\bar{y}}\right)^2+\left(\frac{\partial\bar{u}}{\partial\bar{y}}+\frac{\partial\bar{v}}{\partial\bar{x}}\right)^2\right) + \eta^*\left[\left(\frac{\partial^2\bar{v}}{\partial\bar{x}^2}+\frac{\partial^2\bar{v}}{\partial\bar{y}^2}\right)^2+\left(\frac{\partial^2\bar{u}}{\partial\bar{x}^2}+\frac{\partial^2\bar{u}}{\partial\bar{y}^2}\right)^2\right] + \frac{\rho D K_{\mathrm{T}}}{T_m}\left(\frac{\partial^2 C}{\partial\bar{X}^2}+\frac{\partial^2 C}{\partial\bar{Y}^2}\right), \tag{A13}$$

$$\left(\bar{u}\frac{\partial}{\partial\bar{x}}+\bar{v}\frac{\partial}{\partial\bar{y}}\right)C = D\left(\frac{\partial^2 C}{\partial\bar{x}^2}+\frac{\partial^2 C}{\partial\bar{y}^2}\right)+\frac{DK_{\mathrm{T}}}{T_m}\left(\frac{\partial^2 T}{\partial\bar{x}^2}+\frac{\partial^2 T}{\partial\bar{y}^2}\right). \tag{A14}$$

Introducing the non-dimensional quantities

$$x=\frac{\bar{x}}{\lambda},\ y=\frac{\bar{y}}{d_1},\ u=\frac{\bar{u}}{c},\ v=\frac{\bar{v}}{c\delta},\ p=\frac{d_1^2}{c\mu\lambda}\bar{p},\ h_1=\frac{\bar{h}_1}{d_1},\ h_2=\frac{\bar{h}_2}{d_1},\ \mathbf{S}=\frac{d_1}{\mu c}\bar{\mathbf{S}},$$

$$\eta=\frac{\eta^*}{\mu d_1^2},\ \delta=\frac{d_1}{\lambda},\ \mathrm{Re}=\frac{\rho c d_1}{\mu},\ \mathrm{Fr}=\frac{c^2}{g d_1},\ \kappa=\frac{k_0 c}{\mu d_1},\ \Phi=\frac{d_1^2}{\mu c^2}\bar{\Phi},\ \gamma=\frac{T-T_{\mathrm{a}}}{T_{\mathrm{a}}},$$

$$\mathrm{Ec}=\frac{c^2}{\xi T_a},\ \mathrm{Pr}=\frac{\xi\mu}{k},\ \varphi=\frac{C-C_0}{C_1-C_0},\ \mathrm{Sc}=\frac{\mu}{\rho D},\ \mathrm{Sr}=\frac{\rho D K_T T_{\mathrm{a}}}{\mu T_{\mathrm{m}}(C_1-C_0)},$$

$$M^2=\frac{\sigma^* B_0^2 d_1^2}{\mu},\ \mathrm{Br}=\mathrm{Pr}\,\mathrm{Ec},\ \mathrm{Pe}=\mathrm{RePr},\ \mathrm{Bi}_1=\frac{\eta_1 d_1}{\kappa},\ \mathrm{Bi}_2=\frac{\eta_2 d_1}{\kappa},$$

$$\mathrm{Du}=\frac{\rho D K_{\mathrm{T}}(C_1-C_0)}{\mu\xi c_{\mathrm{s}} T_{\mathrm{a}}}, \tag{A15}$$

the incompressibility condition is automatically satisfied and eqs (A11)–(A14) take the form

$$\delta\mathrm{Re}\left(u\frac{\partial}{\partial x}+v\frac{\partial}{\partial y}\right)u = -\frac{\partial p}{\partial x}+\delta^2\frac{\partial^2 u}{\partial x^2}+\frac{\partial^2 u}{\partial y^2}-\eta\left(\delta^4\frac{\partial^4 u}{\partial x^4}+2\delta^2\frac{\partial^4 u}{\partial x^2\partial y^2}+\frac{\partial^4 u}{\partial y^4}\right)-\frac{M^2}{1+m^2}\cos\theta\,(u\cos\theta-v\delta\sin\theta+\cos\theta)+\frac{\mathrm{Re}\sin\alpha}{\mathrm{Fr}}, \tag{A16}$$

$$\delta^3\mathrm{Re}\left(u\frac{\partial}{\partial x}+v\frac{\partial}{\partial y}\right)v = -\frac{\partial p}{\partial y}+\delta^2\left(\delta^2\frac{\partial^2 v}{\partial x^2}+\frac{\partial^2 v}{\partial y^2}\right)-\eta\delta^2\left(\delta^4\frac{\partial^4 v}{\partial x^4}+2\delta^2\frac{\partial^4 v}{\partial x^2\partial y^2}+\frac{\partial^4 v}{\partial y^4}\right)+\frac{M^2}{1+m^2}\delta\sin\theta\,(u\cos\theta-\delta v\sin\theta+\cos\theta)-\delta\frac{\mathrm{Re}\cos\alpha}{\mathrm{Fr}}, \tag{A17}$$

$$\delta \mathrm{Pe}\left(u\frac{\partial}{\partial x}+v\frac{\partial}{\partial y}\right)\gamma = \delta^2\frac{\partial^2\gamma}{\partial x^2}+\frac{\partial^2\gamma}{\partial y^2}+\mathrm{Br}\left[2\delta^2\left(\frac{\partial u}{\partial x}\right)^2+2\delta^2\left(\frac{\partial v}{\partial y}\right)^2 + \left(\frac{\partial u}{\partial y}+\delta^2\frac{\partial v}{\partial x}\right)^2\right]+\eta\mathrm{Br}\left[\delta^2\left(\delta^2\frac{\partial^2 v}{\partial x^2}+\frac{\partial^2 v}{\partial y^2}\right)^2 + \left(\delta^2\frac{\partial^2 u}{\partial x^2}+\frac{\partial^2 u}{\partial y^2}\right)^2\right]+\mathrm{Pr}\,\mathrm{Du}\left(\delta^2\frac{\partial^2\varphi}{\partial x^2}+\frac{\partial^2\varphi}{\partial y^2}\right), \tag{A18}$$

$$\delta \mathrm{Re}\left(u\frac{\partial}{\partial x}+v\frac{\partial}{\partial y}\right)\varphi = \frac{1}{\mathrm{Sc}}\left(\delta^2\frac{\partial^2\varphi}{\partial x^2}+\frac{\partial^2\varphi}{\partial y^2}\right)+\mathrm{Sr}\left(\delta^2\frac{\partial^2\gamma}{\partial x^2}+\frac{\partial^2\gamma}{\partial y^2}\right), \tag{A19}$$

where Re is the Reynolds number, Fr is the Froude number, Pe is the Peclett number, Br is the Brinkman number, Pr is the Prandtl number, Du is the Dufour number, Sc is the Schmidt number and Sr is the Soret number.

Appendix B

Here constants appearing in the solutions are mentioned as follows:

$$z=\frac{M^2}{1+m^2},\quad H=\frac{M^2}{1+m^2}\cos^2\theta-\frac{\mathrm{Re}}{\mathrm{Fr}}\sin\alpha+\frac{\mathrm{d}p}{\mathrm{d}x},$$
$$A_1=\frac{h_1\sqrt{(A_4/\eta)}}{\sqrt{2}},\quad A_2=\frac{h_2\sqrt{(A_4/\eta)}}{\sqrt{2}},\quad A_3=-1+A_5,\quad A_4=1+A_5,$$
$$A_5=\sqrt{\frac{1+m^2-2M^2\eta-2M^2\eta\cos 2\theta}{1+m^2}},\quad A_6=1+m^2-2M^2\eta\cos 2\theta.$$
$$M_1=\sqrt{-\frac{-1+\sqrt{1-4z\eta\cos^2\theta}}{\eta}},\quad M_2=\sqrt{\frac{1+\sqrt{1-4z\eta\cos^2\theta}}{\eta}},$$
$$M_3=\sqrt{1-4z\eta\cos^2\theta},$$

and the constants C_i ($i = 1$–8) in eqs (15)–(18) can be obtained easily by using the boundary conditions (9) and (10).

References

[1] Kh S Mekheimer, Y Abd elmaboud and A I Abdellateef, *Appl. Biol. Biomech.* **10**, 19 (2013)
[2] Kh S Mekheimer and Y Abd elmaboud, *Appl. Math. Model.* **35**, 2695 (2011)
[3] D Tripathi, *Transp. Porous Med.* **92**, 559 (2012)
[4] S K Pandey and M K Chaube, *Math. Comput. Model.* **52**, 501 (2010)
[5] R Ellahi, A Riaz and S Nadeem, *I. J. Phys.* **87**, 1275 (2013)
[6] R Ellahi, A Riaz and S Nadeem *Appl. Nanosci.* **4**, 753 (2014)
[7] M Kothandapani and S Srinivas, *Phys. Lett. A* **372**, 1265 (2008)

[8] S Nadeem and E N Maraj, *Commun. Theor. Phys.* **59**, 729 (2013)
[9] M H Haroun, *Comput. Mater. Sci.* **39**, 324 (2007)
[10] T Hayat, S Noreen, N Ali and S Abbasbanday, *Inc. Numer. Methods Partial Differential Eq.* **28**, 737 (2012)
[11] T Hayat, S Hina, M Mustafa and A Alsaedi, *J. Heat Transfer* **135**, 041701 (2013)
[12] K Fakhar, A H Kara, R Morris and T Hayat, *Indian J. Phys.* **87**, 1035 (2013)
[13] S Nadeem and S Akram, *Arch. Appl. Mech.* **81**, 97 (2011)
[14] N T Eldabe, S M Elshaboury, A A Hasan and M A Elogail, *Innov. Sys. Design Eng.* **3**, ISSN 2222-2871 (2012)
[15] M Kothandapani, S Srinivas and R Gayathri, *Commun. Nonlinear Sci. Numer. Simulat.* **16**, 1845 (2011)
[16] D Tripathi, S K Pandey and O Anwar Bég, *Int. J. Thermal Sci.* **70**, 41 (2013)
[17] Y Abd elmaboud, *Commun. Nonlinear Sci. Numer. Simulat.* **17**, 685 (2012)
[18] N S Akbar, S Nadeem, R Ul Haq and Z H Khan, *Indian J. Phys.* **87**, 1121 (2013)
[19] S Noreen, T Hayat, A Alsaedi and M Qasim, *Indian J. Phys.* **87**, 889 (2013)
[20] T Hayat, N Ali and S Hina, *Commun. Nonlinear Sci. Numer. Simulat.* **15**, 1526 (2010)
[21] T Hayat, S Noreen, M S Alhothuali, S Asghar and A Alhomaidan, *Int. J. Heat Mass Transfer* **55**, 443 (2012)
[22] T Hayat and S Hina, *Nonlinear Analysis: Real World Applications* **11**, 3155 (2010)
[23] T Hayat, N Ali and S Asghar, *Phys. Lett. A* **363**, 397 (2007)
[24] S R El Koumy, I B El Syed and S I Abdelsalam, *Trans. Porous Med.* **94**, 643 (2012)
[25] M A M Abdeen, H A Attia, W Abbas and W Abd El-Meged, *Indian J. Phys.* **87**, 767 (2013)
[26] T Hayat, F M Abbasi and S Obaidat, *Magnetohydrodynamics* **47**, 295 (2011)
[27] T Hayat, H Yasmin, M S Alhuthali and M A Kutbi, *J. Mech.* **29**, 599 (2013)
[28] T Chinyoka and O D Makinde, *Math. Comput. Model.* **54**, 160 (2011)
[29] A M Abd-Alla, S M Abo-Dahab and R D El-Semiry, *Korea-Australia Rheol. J.* **25**, 107 (2013)
[30] N Ali, Y Wang, T Hayat and M Oberlack, *Biorheol.* **45**, 611 (2008)